Enhanced nondipole effects in photoelectron angular distributions near giant dipole autoionizing resonances in atoms

V. K. Dolmatov,[1,*] A. S. Baltenkov,[2,†] and S. T. Manson[3,‡]
[1]*Department of Physics and Earth Science, University of North Alabama, Florence, Alabama 35632, USA*
[2]*Arifov Institute of Electronics, Akademgorodok, Tashkent 700125, Uzbekistan*
[3]*Department of Physics and Astronomy, Georgia State University, Atlanta, Georgia 30303, USA*
(Received 25 January 2003; revised manuscript received 31 March 2003; published 25 June 2003)

It is found that dipole-quadrupole photoelectron angular distribution parameters in regions of $np \rightarrow nd$ giant dipole resonances in $3d$ $(n=3)$ and $4d$ $(n=4)$ transition-metal atoms are resonantly increased to such an extent that they can dominate the effects of dipole transitions on the asymmetry of the photoelectron angular distribution. This is illustrated for $3d$ photoionization of Cr and Mn, as well as for $4d$ photoionization of Mo and Tc, where the ''spin-polarized'' random-phase approximation with exchange calculations are performed with allowance for correlations in both dipole and quadrupole channels.

DOI: 10.1103/PhysRevA.67.062714 PACS number(s): 32.80.Dz, 32.80.Fb

I. INTRODUCTION

Over the past decade or so, investigations of electric dipole—electric quadrupole ($E1$-$E2$) interference effects in photoelectron angular distributions have been the subject of numerous studies by both experimentalists and theorists. The effect arises from the first-order correction to the dipole approximation for a photoionization matrix element between the initial and the final states: $M_{if}=(f|(1+i\mathbf{k}\cdot\mathbf{r})\mathbf{e}\cdot\mathbf{p}|i)$, with $\mathbf{k}$ and $\mathbf{e}$ being the photon momentum (in atomic units) and polarization vector, and $\mathbf{r}$ and $\mathbf{p}$ being the electron position vector and the electron momentum operator. The correction term $i\mathbf{k}\cdot\mathbf{r}$ in this expression gives rise to the appearance of the electric $E1$-$E2$ interference term in the differential photoionization cross section $d\sigma_{nl}/d\Omega$ of a nl subshell of the atom. These studies have quickly been extended from atoms to molecules [1,2] and solids [3], as well as to magnetic dichroism in atomic photoionization [6], and have bridged the gap between the studies of spin-averaged and spin-resolved photoelectron angular distributions, including the $E1$-$E2$ interference [4,5].

The upsurge in modern studies of the nondipole parameters γ_{nl} and δ_{nl} was stimulated primarily by an experiment that, owing to the advances in synchrotron and detector technology, has demonstrated that the laboratory measurement of γ_{nl} and δ_{nl}, the nondipole photoelectron angular distribution parameters, is now quite feasible in the photon energy range of not only thousands of eV or more, but of hundreds and even tens of eV as well [7]. Unexpectedly, these parameters have been found, in many cases, both experimentally and theoretically significant, comparable to (or even larger than) β_{nl}, the purely dipole photoelectron angular distribution asymmetry parameter. This is of importance since the dipole contributions used to be thought as the only determinants of the photoionization process at photon energies below a few thousands of eV.

Owing to the findings of recent years, thus, the era of tacit belief that nondipole $E1$-$E2$ interference effects are undetectable against the background of pure dipole effects at low photon energies, including energies as low as tens of eV, is over. As a consequence, the number of both experimental and theoretical studies in the area of nondipole contributions to photoelectron angular distributions has grown rapidly in the recent years.

In light of recent advances showing the significant strength of $E1$-$E2$ interference effects at low (tens of eV) and relatively low (hundreds to a few thousands of eV) photon energies, the search for situations where nondipole effects are particularly strong, compared to pure dipole effects, has become a task of importance. Such a situation occurs, e.g., when the dominant dipole photoionization amplitude exhibits a Cooper minimum [8,9]. Other situations occur when there is a strong autoionizing resonance in a *quadrupole* or *dipole* photoionization amplitude [10,11,20], a quadrupole resonance in *continuous* spectrum [12], or a quadrupole quasiresonance in a confined atom [13]. The investigation of other situations where nondipole effects are strong remains, however, of interest.

The aim of the present paper is to show that the nondipole $E1$-$E2$ interference effects can be comparable to, or bigger than, the dipole $E1$-$E1$ effect in regions of dipole $np \rightarrow nd$ autoionizing resonances in $3d$ $(n=3)$ and $4d$ $(n=4)$ transition-metal atoms. These resonances, as was detailed earlier for the Cr and Mn atoms (see, e.g., Refs. [14–16] and references therein), are giant resonances in terms of their large oscillator strengths, along with large widths associated with the decay into primarily the $nd \rightarrow \epsilon f, \epsilon p$ continuum. The drastic enhancement in the $E1$-$E2$ interference effects near the giant resonances is illustrated by the calculations of both the dipole β_{nl} and the nondipole γ_{nl} and δ_{nl} angular distribution parameters for $3d$ photoelectrons from the Cr and Mn atoms, as well as for $4d$ photoelectrons from the Mo and Tc atoms.

The Cr, Mn, Mo, and Tc atoms were chosen because they are the simplest representatives of the $3d$ and $4d$ transition metals, since they contain only one [in Mn ($3d^5$) and

*Electronic address: vkdolmatov@una.edu
†Electronic address: arkadiy@ariel.tashkent.su
‡Electronic address: smanson@gsu.edu

Tc ($4d^5$)] or two [in Cr ($3d^5 4s^1$) and Mo ($4d^5 5s^1$)] half-filled subshells, with all the other subshells closed. This makes it possible to apply the ''spin-polarized'' random-phase approximation with exchange (SPRPAE) [16,17] for calculations of photoionization parameters for such atoms. SPRPAE accounts for a significant part of the correlation, including interchannel coupling between photoionization channels, which is crucial for the description of resonance photoionization. Earlier studies, using this methodology, allowed us to understand very well, both qualitatively and quantitatively, the $3p \rightarrow 3d$ dipole giant resonances in the $3d$ photoionization of both the Mn [16] and the Cr [15,18] atoms. We expect this method to be applicable equally well to the corresponding $4d$ elements, Mo and Tc.

II. THEORY

The $E1$-$E2$ interference effects are represented by the appearance of the so-called nondipole γ_{nl} and δ_{nl} parameters, in addition to the dipole β_{nl} parameter, in the differential photoionization cross section $d\sigma_{nl}/d\Omega$ of a nl subshell with accounting for the lowest-order $E1$-$E2$ correction. Explicit expressions for $d\sigma_{nl}/d\Omega$ have been given for unpolarized light [19], for 100% linearly polarized light [20,21], and for general polarization [22]. For 100% linearly polarized light,

$$\frac{d\sigma_{nl}}{d\Omega} = \frac{\sigma_{nl}}{4\pi}\left[1 + \frac{\beta_{nl}}{2}(3\cos^2\theta - 1)\right] + \Delta E_{12}. \tag{1}$$

Here σ_{nl} is the dipole photoionization cross section of the subshell nl, β_{nl} is the dipole photoelectron angular asymmetry parameter, and ΔE_{12} is the $E1$-$E2$ interference correction term:

$$\Delta E_{12} = \frac{\sigma_{nl}}{4\pi}(\delta_{nl} + \gamma_{nl}\cos^2\theta)\sin\theta\cos\phi, \tag{2}$$

where the spherical angles θ and ϕ are defined in relation to the directions of the photon momentum **k**, photoelectron momentum **p**, and photon polarization vector **e**; and β_{nl}, γ_{nl}, and δ_{nl} are

$$\beta_{nl} = \frac{l(l-1)d_{l-1}^2 + (l+1)(l+2)d_{l+1}^2}{(2l+1)[ld_{l-1}^2 + (l+1)d_{l+1}^2]} - \frac{6l(l+1)d_{l-1}d_{l+1}\cos(\delta_{l+1} - \delta_{l-1})}{(2l+1)[ld_{l-1}^2 + (l+1)d_{l+1}^2]}, \tag{3}$$

$$\gamma_{nl} = \frac{3k}{2[ld_{l-1}^2 + (l+1)d_{l+1}^2]} \sum_{l',l''} A_{l',l''} d_{l'} q_{l''} \cos(\delta_{l''} - \delta_{l'}), \tag{4}$$

$$\delta_{nl} = \frac{3k}{2[ld_{l-1}^2 + (l+1)d_{l+1}^2]} \sum_{l',l''} B_{l',l''} d_{l'} q_{l''} \cos(\delta_{l''} - \delta_{l'}). \tag{5}$$

Here $d_{l'}$ and $q_{l''}$ are the radial dipole and quadrupole photoionization amplitudes, respectively, given by

$$d_{l'} = \int_0^\infty P_{\epsilon l'}(r) r P_{nl}(r) dr, \tag{6}$$

$$q_{l''} = \int_0^\infty P_{\epsilon l''}(r) r^2 P_{nl}(r) dr, \tag{7}$$

where $P_{nl}(r)/r$ and $P_{\epsilon\lambda}(r)/r$ are the radial parts of the electron wave functions in the bound nl state and in the continuous $\epsilon\lambda$ spectrum, respectively. $l' = l \pm 1$, $l'' = l, l \pm 2$, and δ_λ are the phase shifts of the wave functions of photoelectrons in the field of the positive ionic core, and coefficients $A_{l',l''}$ and $B_{l',l''}$ are given in Ref. [21].

The above equations define the β_{nl}, γ_{nl}, and δ_{nl} asymmetry parameters in a single-electron approximation. However, because the aim of this paper is to investigate these parameters in the autoionizing resonance domain, these equations must be generalized to include interchannel interactions or, in general terms, electron-electron correlation. The generalization of these equations beyond a single-electron approximation is simple [19]; the single-electron matrix elements $d_{l'}$ and $q_{l''}$ must be replaced by, generally complex, matrix elements calculated with account for the electron correlation, $D_{l'}$ and $Q_{l''}$, respectively, i.e., $d_{l'} \rightarrow D_{l'}$, $q_{l''} \rightarrow Q_{l''}$, along with the following replacements:

$$d_\lambda^2 \rightarrow |D_{\lambda'}|^2,$$

$$d_\lambda t_{\lambda'} \cos\Delta\delta \rightarrow (D'_\lambda, T'_{\lambda'} + D''_\lambda, T''_{\lambda'})\cos\Delta\delta + (D''_\lambda, T'_{\lambda'} - D'_{l'} T''_{\lambda'})\sin\Delta\delta,$$

$$\Delta\delta = \delta_{\lambda'} - \delta_\lambda, \tag{8}$$

where $t(T)$ stands either for a quadrupole matrix element $q(Q)$ or a dipole matrix element $d(D)$, D' and Q' are the real parts of corresponding matrix elements, whereas D'' and Q'' are their imaginary parts.

In this paper, to account for the electron correlation (interchannel interaction) in photoionization matrix elements, we use the SPRPAE [16,17] which is a generalization of standard RPAE [23] to atoms with half-filled subshells, since atoms of our choice—Cr, Mn, Mo, and Tc—are just these types of atoms. Both approximations, RPAE and SPRPAE, are described in detail in the above references. Here, the discussion is limited to the aspects, of these methods, of direct relevance to calculations of the present paper.

The SPRPAE uses spin-polarized Hartree-Fock (SPHF) [24] wave functions and energies as the zero-order basis. In SPHF, the ground-state configuration of Mn ($n=3$) and Tc ($n=4$) is $\ldots np^3\uparrow np^3\downarrow nd^5\uparrow (n+1)s^1\uparrow (n+1)s^1\downarrow (^6S)$, where arrows $\uparrow$ and $\downarrow$ correspond to the *up* and *down* orientations of the electronic spin, the spins of all five nd^5 electrons are parallel according to the Hund's rule. The ground-state configuration of the Cr ($n=3$) and Mo ($n=4$) atoms, whose outermost $(n+1)s$ subshells are half-filled subshells as well, differ from the above configuration by the absence of the $(n+1)s\downarrow$ electron: $\ldots np^3\uparrow np^3\downarrow nd^5\uparrow (n+1)s^1\uparrow (^7S)$. Each closed subshell is,

thus, separated into two, spin-up and spin-down, subshells. Both the energies and the wave functions of spin-up and spin-down electrons with the same n's and l's are different due to the presence (absence) of exchange interaction between spin-up (spin-down) electrons with only spin-up electrons from the $nd^5\uparrow$ (as well as from $4s^1\uparrow$ in Cr and Mo) half-filled subshell(s).

Within the above approach, the giant dipole $np\rightarrow nd$ autoionizing resonances in the Cr, Mn, Mo, and Tc atoms are formed by the $np\downarrow\rightarrow nd\downarrow$ photoexcitations of the $np\downarrow$ electron into the empty $nd\downarrow$ state. Such excited states decay rapidly primarily into the continuous spectrum of the $nd^5\uparrow$ subshell, resulting in the appearance of the giant autoionizing resonances in the np absorption spectra of these atoms. Besides, for Cr and Mo, an additional $np\downarrow\rightarrow(n+1)s\downarrow$ autoionizing transition is possible, owing to the half-filled outermost $(n+1)s$ subshells, making their resonance spectra more complicated than those of Mn and Tc.

To describe such spectra, one must account for the interchannel interactions (electron correlation) between the groups of transitions with various mutual spin orientations (up-up, up-down, down-up, and down-down). The SPRPAE [16,17] provides a way for accounting for such interchannel interactions in half-filled subshell atoms, within the general methodology of RPAE. Note that similar to RPAE, SPRPAE omits spin-spin and spin-orbit interactions in the atom, and hence spin-flip transitions are excluded from consideration within SPRPAE. More detail is given elsewhere [16,17]. As noted in the Introduction, SPRPAE was tested by the application to the investigation of the giant resonances in the Mn and Cr atoms, and the results obtained were proven to be a success, speaking of the credibility of SPRPAE.

In the present work, the calculations of the photoionization matrix elements included coupling among all initial-state and final-state single excitation channels, arising from the np, nd, and $(n+1)s$ subshells, in both dipole and quadrupole manifolds (of course, no coupling exists between dipole and quadrupole photoionization channels): $[np\downarrow\rightarrow nd\downarrow,\epsilon d\downarrow]$, $[nd\uparrow\rightarrow n'l'\uparrow,\epsilon l'\uparrow]$, $[(n+1)s\uparrow\rightarrow n''l''\uparrow,\epsilon l''\uparrow]$, and $[(n+1)s\downarrow\rightarrow nl''\downarrow,\epsilon l''\downarrow]$ (when the latter existed). Interchannel interactions with deeper subshells of these atoms were found to be negligibly small in the energy range under discussion. In all cases, it was found that for the dipole manifold, the $np\downarrow$ channels affect the $nd\uparrow$ channels very significantly, resulting in appearance of the giant dipole resonances in dipole photoionization amplitudes D_{nd} and cross sections. However, no significant interchannel coupling was evident for the quadrupole photoionization amplitudes Q_{nd} in the quadrupole manifold in the energy range under discussion.

Our trial calculations showed that, with the exception for the Cr atom, the ''frozen-core'' approximation is a good approximation for the calculations of SPHF wave functions of excited states in Mn, Mo, and Tc. Correspondingly, the frozen-core wave functions were used in SPRPAE calculations of nd photoelectron angular asymmetries from these atoms.

In contrast, the Cr atom, however, was shown earlier [15,18,26] to be the most unusual of the $3d$ atoms because its $3d\downarrow$ and $4d\downarrow$ excited (autoionizing) orbitals (due to $3p\downarrow\rightarrow 3d\downarrow\ ^7P$ and $3p\downarrow\rightarrow 4d\downarrow\ ^7P$ autoionizing excitations) are subject to incomplete (partial) relaxation. The idea behind the incomplete-relaxation phenomenology is that it assumes that the lifetime of the Cr $3p\downarrow\rightarrow 3d,4d\downarrow^7P$ resonances is comparable with the time scale of relaxation of the atomic core upon these excitations, so that the autoionizing decay of the excited states occurs while the relaxation of the atomic core is in progress. Correspondingly, in the present paper, these excited autoionizing orbitals of Cr, $3d\downarrow$ and $4d\downarrow$, were calculated within the framework of the incomplete-relaxation phenomenology, exactly in the same manner as was done earlier [15,18], since the way was proven to be a success. The above references detail the phenomenology of incomplete relaxation by the $3d\downarrow$ and $4d\downarrow$ excited orbitals in Cr.

Another feature of the Cr atom is that its $3p\downarrow\rightarrow 4d\downarrow\ ^7P$ and $3p\downarrow\rightarrow 4s\downarrow\ ^7P$ excited states are well multiplet split into $^7P_{2,3,4}$ terms, characterized by different values of the total momentum $J=2,3,4$ [25]. However, the SPHF approximation, and hence SPRPAE, either does not account for multiplet splitting of the LS terms. To correct for that, exactly in the same manner as was done earlier [15,18], we use the same J-averaged SPHF wave functions for all the multiplet-split components, but substitute the corresponding experimental energies $\omega_{iJ}^{expt.}$ [15] for the different J components of the related ith resonance into the final SPRPAE equations. Since resonances for different J do not interfere, the photoionization cross section $\sigma_{3d}(\omega)$ and the asymmetry parameters $\beta_{3d}(\omega)$, $\gamma_{3d}(\omega)$, and $\delta_{3d}(\omega)$ (ω being the photon frequency) are given by

$$\sigma_{3d}(\omega)=\sum_J \sigma_J(\omega), \tag{9}$$

$$\sigma_J(\omega)=\frac{2J+1}{(2L+1)(2S+1)}\sigma_{3d}(\omega,\omega_{i_J}^{expt.}), \tag{10}$$

$$\sigma_{3d}(\omega,\omega_{i_J}^{expt.})=\frac{4\pi^2\alpha a_0^2}{3}\omega\left|D_{3d}(\omega,\omega_{i_J}^{expt.})\right|^2, \tag{11}$$

$$F_{3d}(\omega)=\sum_J \frac{F_{3d}(\omega,\omega_{i_J}^{expt.})\sigma_{3d}(\omega,\omega_{i_J}^{expt.})}{\sigma_{3d}(\omega)}. \tag{12}$$

Here, J ($J=2,3,4$), L ($L=1$), and S ($S=7$) are, respectively, the total momentum, the total orbital momentum, and the total spin of i's autoionizing excited state (i.e., of one of the $3p\downarrow\rightarrow 4s\downarrow$, $3p\downarrow\rightarrow 3d\downarrow$, $3p\downarrow\rightarrow 4d\downarrow$, and $3p\downarrow\rightarrow 5d\downarrow$ autoionizing resonances). Also, α is the fine-structure constant; a_0 is the first Bohr radius; $D_{3d}(\omega,\omega_{i_J}^{expt.})$ is the SPRPAE dipole photoionization amplitude of the $3d^5\uparrow$ subshell of Cr taken in the length form and calculated in the energy range of the autoionizing resonance multiplet-split components considered for each J; F_{3d} stands for either β_{3d}, γ_{3d}, or δ_{3d} photoelectron asymmetry parameter, respectively; and $F_{3d}(\omega,\omega_{i_J}^{expt.})$ is the corresponding asymmetry parameter calculated for each final J channel.

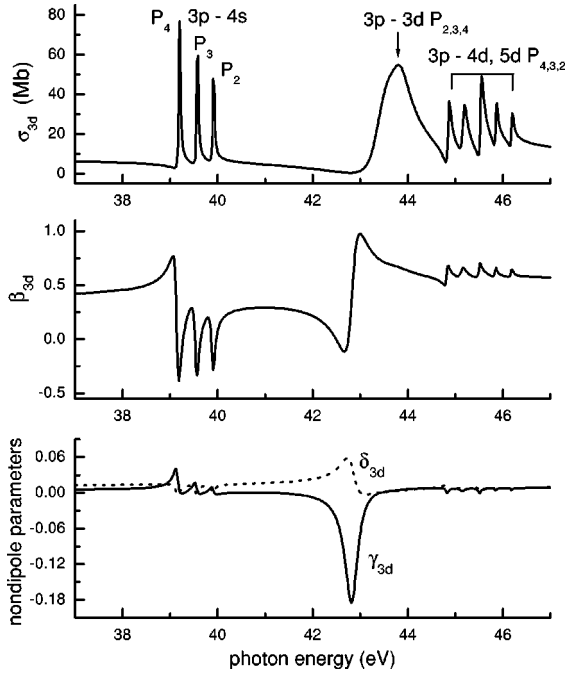

FIG. 1. SPRPAE calculations of the Cr $3d$ photoionization cross section σ_{3d}, as well as the dipole β_{3d} and nondipole γ_{3d} and δ_{3d} photoelectron angular distribution parameters in the vicinity of the $3p \rightarrow 4s$, giant $3p \rightarrow 3d$, and Rydberg $3p \rightarrow 4d,5d$ autoionizing resonances.

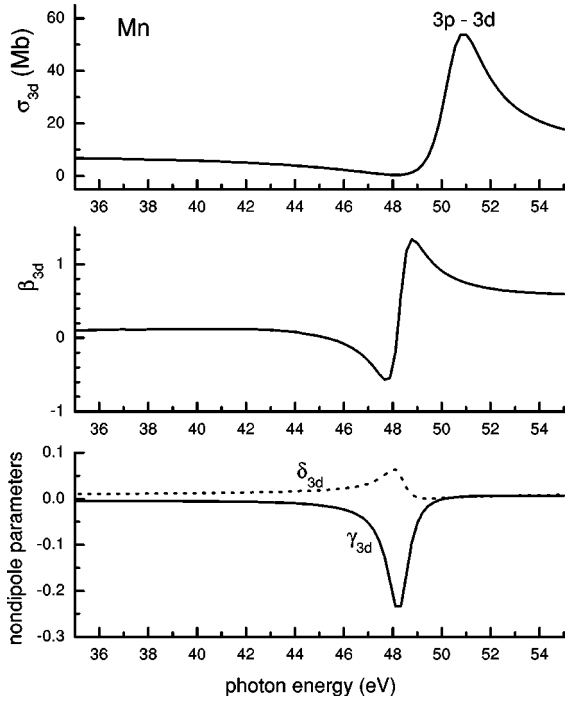

FIG. 2. SPRPAE calculations of the Mn $3d$ photoionization cross section σ_{3d}, as well as the dipole β_{3d} and nondipole γ_{3d} and δ_{3d} photoelectron angular distribution parameters in the vicinity of the dipole giant $3p \rightarrow 3d$ autoionizing resonance.

SPRPAE-calculated results for both $nd\uparrow$ photoelectron angular-asymmetry parameters and dipole photoionization cross sections of Cr, Mn, Mo, and Tc, below the $np\downarrow$ ionization threshold, are presented and considered in the following section. Note that everywhere below, for the sake of simplicity, when it is not confusing, we omit spin-indicating arrows $\uparrow$ and $\downarrow$.

III. RESULTS AND DISCUSSION

A. 3*d* photoelectron angular distributions from Cr and Mn

We first focus on β_{3d}, γ_{3d}, and δ_{3d} angular-asymmetry parameters for $3d$ photoelectrons from Cr, below the $3p\ ^7P_{2,3,4}(3p\downarrow)$ ionization threshold. Note that, to the best of our knowledge, the dipole angular-asymmetry parameter β_{3d} of Cr, in the resonance energy range under discussion, has not been investigated experimentally.

Displayed in Fig. 1 are the results of our SPRPAE calculations for the partial $3d$ photoionization cross section σ_{3d}, as well as for the parameters β_{3d}, γ_{3d}, and δ_{3d}, calculated in the vicinity of dipole $3p \rightarrow 4s$ ($^7P_{2,3,4}$) as well as $3p \rightarrow n(\geqslant 3)d$ ($^7P_{2,3,4}$) autoionizing resonances in Cr. The outstanding feature of the results, relevant to this paper, is the nondipole γ_{3d} parameter which is significantly enhanced in magnitude, as is β_{3d}, just below the $3p \rightarrow 3d$ giant resonance in the photoionization cross section σ_{3d}. In this region, $|\gamma_{3d}|$ has a maximum magnitude of about 0.18, which is extremely large for a nondipole parameter at such a low energy and is comparable to the magnitude of the dipole angular-asymmetry parameter $|\beta_{3d}| \approx 0.12$ at photon energies around 42.8 eV, a clear demonstration of a strong nondipole effect at photon energies as low as a few tens of eV.

In contrast to the $3p \rightarrow 3d$ resonance, the other resonances in Cr are well separated into the three $^7P_4$, $^7P_3$, and $^7P_2$ multiplet components [14]. This, however, tends to dilute the interchannel effects of the multiplet-split resonance components in the photoelectron angular distributions [27]. For this reason, the $3p \rightarrow 4s$ and $3p \rightarrow n(\geqslant 4)d$ resonance structures in the nondipole parameters of Cr are quite weak.

Looking at Mn, where the same channels as in the Cr case are coupled together in the SPRPAE calculation, the calculated data for σ_{3d}, β_{3d}, γ_{3d}, and δ_{3d}, are displayed in Fig. 2. In contrast to the Cr atom, there is no $3p \rightarrow 4s$ resonance in the Mn ($3p^6 3d^5 4s^2$) spectrum because its $4s^2$ subshell is closed. In addition, the $3p \rightarrow (n \geqslant 4)d$ resonances in Mn are weak and located some ten eV higher than the giant $3p \rightarrow 3d$ resonance [14]. As in the Cr case, within the dipole manifold, only the interchannel coupling with $3p$ channels affects the $3d$ amplitudes significantly and, in the quadrupole manifold, interchannel coupling is unimportant.

Of primary interest and importance is the fact that the $|\gamma_{3d}|$ parameter maximizes to approximately 0.25 at a photon energy of about of 48 eV. Not only is the nondipole parameter large in an absolute sense, but it is also of the same size as the dipole parameter β_{3d} in the region of the resonance enhancement. Also of importance is the fact that the energy region where the γ_{3d} parameter is large has a width of nearly 1 eV. This should make the structure in γ_{3d}, owing to the autoionizing resonance, eminently suitable for experimental scrutiny. A similar result was obtained in Ref. [20] using a simplified two-channel version of SPRPAE.

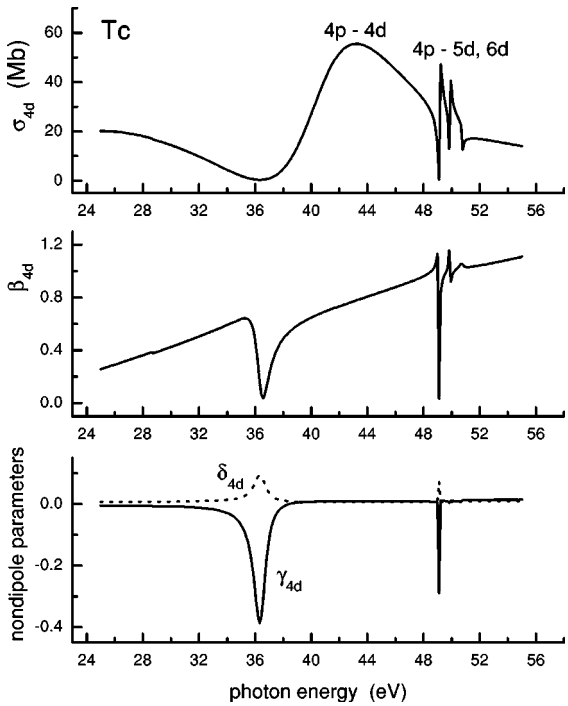

FIG. 3. SPRPAE calculations of the Tc $4d$ photoionization cross section σ_{4d}, as well as the dipole β_{4d} and nondipole γ_{4d} and δ_{4d} photoelectron angular distribution parameters in the vicinity of the dipole giant $4p \rightarrow 4d$ autoionizing resonance.

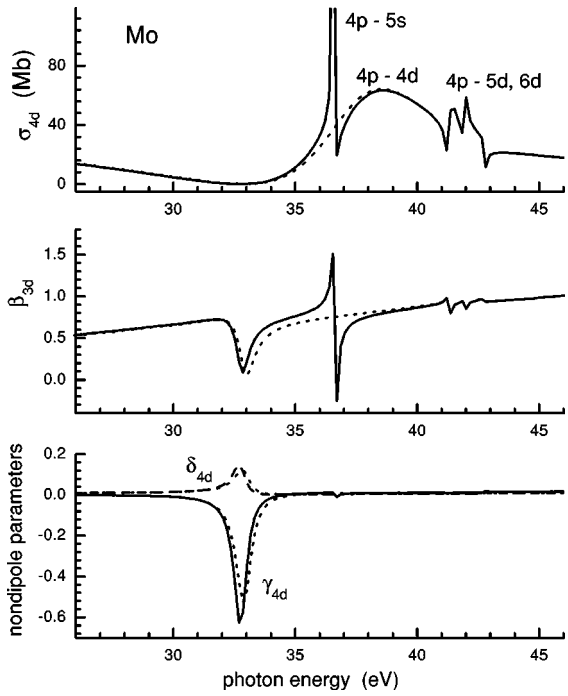

FIG. 4. SPRPAE calculations of the Mo $4d$ photoionization cross section σ_{4d}, as well as the dipole β_{4d} and nondipole γ_{4d} and δ_{4d} photoelectron angular distribution parameters in the vicinity of the $4p \rightarrow 5s$, giant $4p \rightarrow 4d$, and Rydberg $4p \rightarrow 5d,6d$ autoionizing resonances. The dotted lines are SPRPAE calculations with the $4p \rightarrow 5s$ resonance omitted.

B. 4*d* photoelectron angular distributions from Tc and Mo

For the $4d$ equivalents of Cr and Mn, the Mo and Tc atoms, respectively, similar calculations were carried out, except that the coupling among the channels originating from $4p$, $4d$, and $5s$ subshells was treated, both dipole and quadrupole manifolds. Similar to the $3d$ cases, in the dipole channels there is a strong interchannel coupling effect on the $4d$ amplitudes by the $4p$ autoionizing resonance channels, and negligible interchannel coupling was exhibited among quadrupole channels.

We focus first on Fig. 3 that shows resonance variations in β_{4d}, γ_{4d}, and δ_{4d} for the Tc ($4p^6 4d^5 5s^2$) atom at photon energies around 36 eV, i.e., the variations located in a region of the $4p \rightarrow 4d$ giant resonance minimum in the $4d$ photoionization cross section.

Near 36 eV, the magnitude of the $|\gamma_{4d}|$ nondipole parameter is seen to reach a very large value, approximately 0.4, thus making the nondipole effects on the asymmetry of the photoelectron distribution quite competitive with the dipole effects near 36 eV. As for the resonance structures seen above 48 eV, they are the result of the $4p \rightarrow 5d,6d$ autoionizing resonances that are not treated accurately in this calculation, owing to the omission of multiplet splitting; we include them only to show the order of magnitude of their effect on the photoionization parameters.

We now turn to the Mo ($4p^6 4d^5 5s^1$) atom. This atom has a half-filled $5s$ subshell that opens way for a resonance transition $4p \rightarrow 5s$, which occurs rather close to the giant resonance transition $4p \rightarrow 4d$. The presence of the $4p \rightarrow 5s$ resonance, however, as will be seen below, influences very weakly the dipole β_{4d} and nondipole γ_{4d} and δ_{4d} parameters in the photon energy region of the strong structure in the nondipole parameters. We, therefore, simplified the calculations by ignoring the detailed account for the $4p \rightarrow 5s$ resonance, such as multiplet and spin-orbit splitting, in the calculations of β_{4d}, γ_{4d}, and δ_{4d} at photon energies in the vicinity of the structure in the nondipole γ_{4d} and δ_{4d} parameters. Besides, similar to the case of Tc, the higher-lying dipole autoionizing resonances $4p \rightarrow 5d,6d$ have negligible influence on γ_{4d}, and δ_{4d} in the region of structure, so that these are also treated simply, as in the case of Tc. With the above calculational simplifications, our results for σ_{4d}, β_{4d}, γ_{4d}, and δ_{4d} for $4d$ photoionization of the Mo atoms in the vicinity, of the giant $4p \rightarrow 4d$ resonance are shown.

Of greatest significance is the photon energy region around 32.5 eV, where δ_{4d} and, even more so, γ_{4d} are dramatically increased by dipole interchannel coupling, with $|\gamma_{4d}|$ reaching a magnitude of about 0.6, significantly larger than β_{4d} at these energies. This means that the asymmetry of the $4d$ photoelectron angular distribution here is dominated by nondipole effects.

To investigate the approximation made for the treatment of the $4p \rightarrow 5s$ resonance for both dipole β_{4d} and nondipole-γ_{4d} and δ_{4d} photoelectron angular distribution parameters at photon energies near 32.5 eV, where γ_{4d} and δ_{4d} exhibit the significant structure induced by interchannel coupling, we show in Fig. 4 the results of SPRPAE calculations with and without including the $4p \rightarrow 5s$ resonance in the calculations. Clearly, the influence is seen to be negligible for γ_{4d} and

δ_{4d}, and very weak for β_{4d} (at about 32.5 eV), which demonstrates that accurate accounting for the $4p \rightarrow 5s$ resonance is not important. Similarly, the structure in γ_{4d} and δ_{4d} is largely unaffected, with or without the inclusion of the $4p \rightarrow 5d,6d$ resonances in the calculation (not shown). However, the $4p \rightarrow 5s$ and $4p \rightarrow 5d,6d$ resonances are seen to influence β_{4d} and σ_{4d} beyond 35 eV strongly. Thus, the structures seen in β_{4d} and σ_{4d} at about 37 eV and around 42 eV must be considered only qualitative.

IV. CONCLUSION

Calculations have been performed, which provide insight into nondipole effects near dipole giant autoionizing resonances in $3d$ and $4d$ transition-metal atoms. It has been found that nondipole effects in photoelectron angular distributions are dramatically enhanced in such photon energy regions. This has been demonstrated for typical representatives of the $3d$ (Cr and Mn) and $4d$ (Mo and Tc) transition-metal atoms in the region of the $np \rightarrow nd$ giant dipole resonances. Most importantly, the calculations have found that at photon energies near giant resonances (a few tens of eV), γ_{nd} becomes even more important than β_{nd} in the asymmetry of the nd photoelectron angular distribution, a clear demonstration of a case where the dipole approximation alone is expected to fail in understanding angular-asymmetry distributions of photoelectrons, even at such low photon energies.

ACKNOWLEDGMENTS

This work was supported in part by the US Civilian Research and Development Foundation for the Independent States of the Former Soviet Union (CRDF), Grant No. ZP1-2449-TA-02, as well as by NSF and NASA. We are grateful to Professor M. Ya. Amusia and Professor L. V. Chernysheva for the use of their computer codes similar to codes of Ref. [28].

[1] B. Krässig, M. Jung, D.S. Gemmell, E.P. Kanter, T. LeBrun, S.H. Southworth, and L. Young, Phys. Rev. Lett. **75**, 4736 (1995).
[2] D.W. Lindle and O. Hemmers, J. Electron Spectrosc. Relat. Phenom. **100**, 297 (1999).
[3] G.J. Jackson, B.C.C. Cowie, D.P. Woodruff, R.G. Jones, M.S. Kariapper, C. Fisher, A.S.Y. Chan, and M. Butterfield, Phys. Rev. Lett. **84**, 2346 (2000).
[4] A. Bechler and R.H. Pratt, J. Phys. B **32**, 2889 (1999).
[5] N.A. Cherepkov and S.K. Semenov, J. Phys. B **34**, L211 (2001).
[6] A.N. Grum-Grzhimailo, J. Phys. B **34**, L359 (2001).
[7] N.L.S. Martin, D.B. Thompson, R.P. Bauman, C.D. Caldwell, M.O. Krause, S.P. Frigo, and M. Wilson, Phys. Rev. Lett. **81**, 1199 (1998).
[8] W.R. Johnson and K.T. Cheng, Phys. Rev. A **63**, 022504 (2001).
[9] M.Ya. Amusia, A.S. Baltenkov, L.V. Chernysheva, Z. Felfli, and A.Z. Msezane, Phys. Rev. A **63**, 052506 (2001).
[10] V.K. Dolmatov and S.T. Manson, Phys. Rev. Lett. **83**, 939 (1999).
[11] B. Krässig, E.P. Kanter, S.H. Southworth, R. Guillemin, O. Hemmers, D.W. Lindle, R. Wehlitz, and N.L.S. Martin, Phys. Rev. Lett. **88**, 203002 (2002).
[12] N.A. Cherepkov and S.K. Semenov, J. Phys. B **34**, L495 (2001).
[13] J.-P. Connerade, V.K. Dolmatov, and S.T. Manson, J. Phys. B **33**, L275 (2000).
[14] B. Sonntag and P. Zimmermann, Rep. Prog. Phys. **55**, 911 (1992).
[15] Th. Dohrmann, A. von dem Borne, A. Verweyen, B. Sonntag, M. Wedowski, K. Godehusen, P. Zimmermann, and V. Dolmatov, J. Phys. B **29**, 4641 (1996).
[16] M.Ya. Amusia, V.K. Dolmatov, and V.K. Ivanov, Zh. Éksp. Teor. Fiz. **85**, 115 (1983) [Sov. Phys. JETP **58**, 67 (1983)].
[17] M.Ya. Amusia and V.K. Dolmatov, J. Phys. B **26**, 1425 (1993).
[18] V.K. Dolmatov, J. Phys. B **26**, L393 (1993).
[19] M.Ya. Amusia, P.U. Arifov, A.S. Baltenkov, A.A. Grinberg, and S.G. Shapiro, Phys. Lett. **47A**, 66 (1974).
[20] M.Ya. Amusia, V.K. Dolmatov, and V.K. Ivanov, Zh. Tekh. Fiz. **56**, 8 (1986) [Sov. Phys. Tech. Phys. **31**, 4 (1986)].
[21] J.W. Cooper, Phys. Rev. A **47**, 1841 (1993). Note that in Table XII the coefficient $A_{l+1,l-2}$ has the incorrect sign.
[22] P.S. Shaw, U. Arp, and S.H. Southworth, Phys. Rev. A **54**, 1463 (1996).
[23] M. Ya Amusia, *Atomic Photoeffect* (Plenum, New York, 1990).
[24] J. Slater, *Self-Consistent Fields for Molecules and Solids* (McGraw-Hill, New York, 1974).
[25] J.T. Costello, E.T. Kennedy, B.F. Sonntag, and C.W. Clark, Phys. Rev. A **43**, 1441 (1991).
[26] V.K. Dolmatov, J. Phys. B **26**, L585 (1993).
[27] V.K. Dolmatov and S.T. Manson, J. Phys. B **30**, L517 (1997).
[28] M.Ya. Amusia and L.V. Chernysheva, *Computation of Atomic Processes* (IOP Publishing Ltd., Bristol, 1997).